J. Fluid Mech. (1975), *vol.* 70, *part* 4, *pp.* 773–799
Printed in Great Britain

Transition in a two-dimensional plane wall jet

By R. A. BAJURA AND M. R. CATALANO†

Department of Mechanical Engineering and Mechanics,
West Virginia University, Morgantown, West Virginia 26506

(Received 7 August 1974)

Transition in a two-dimensional plane wall jet was examined for the range of exit Reynolds numbers between 100 and 600. The wall jet was produced by the flow of water, which issued either from a smoothly-contoured nozzle or from the end of a long parallel channel. Observations were recorded both visually and with a hot-film anemometer. Both natural and forced transition cases were studied. Natural transition generally occurred in the following stages: (i) formation of discrete vortices in the outer shear layer; (ii) coalescence of adjacent vortices in the outer shear layer, coupled with the rolling up of the inner shear layer; (iii) eruption of the wall jet off the surface of the flat plate into the ambient fluid; (iv) dispersion of the organized flow pattern by three-dimensional turbulent motions; and (v) re-laminarization of the upstream flow, until another vortex pairing occurred. The initial stages of transition are two-dimensional in nature; and are dominated by the mechanism of vortex pairing, which is commonly observed in free shear layers. The inner-region shear layer exerts a stabilizing influence on the velocity profile at low Reynolds numbers. Forced transition was essentially similar to natural transition, except for the elimination of the downstream intermittency and the establishment of a fixed downstream location for transition.

1. Introduction

The plane wall jet velocity profile contains two distinct boundary-layer flow regimes. The portion of the flow field between the surface and the point of maximum velocity is called the *inner region*; and it is similar to a wall boundary layer. The remainder of the flow field, called the *outer region*, is similar to the shear layer in a plane free jet. The laminar–turbulent transition processes for simpler flows corresponding to the inner and outer regions have been studied in detail. Transition in a wall boundary layer is characterized by the three-dimensional deformation of Tollmien–Schlichting waves, and the creation of turbulent spots, owing to the subsequent stretching and breakdown of vortex lines associated with the disturbance. Transition in unbounded shear layers, such as in jets and wakes, is characterized by the coalescence of adjacent vortices owing to mutual induction in a distinctly two-dimensional motion and a subsequent breakdown of the flow into turbulence. In a mixed flow field, such as the

† Present address: Engineering Division, Rohm-Haas Company, Bristol, Pa. 19007.

plane wall jet, it might be expected that the viscous effects due to the bounding wall would have a stabilizing influence on the outer region. Conversely, by applying the point-of-inflexion criterion to the velocity profile as a whole, the flow in the inner region would be destabilized by disturbances arising in the outer region. The present study was undertaken to determine the initial transition characteristics of both the inner and outer regions, and the interaction of these two regions in later stages of transition. The present results were then compared with the transitions observed in the basic flows corresponding to the inner and outer regions, to determine which instability mechanism had the greatest effect on the wall jet transition process.

2. Literature

2.1. *Plane wall jets*

Laminar wall jets, moving parallel to a flat surface, were treated theoretically by Tetervin (1948) and Glauert (1956). Similarity solutions for wall jets flowing along curved surfaces were obtained by Wygnanski & Champagne (1968), Parks & Petersen (1968), Lindow & Greber (1968) and Mon (1970). Experimental studies of laminar wall jets were conducted by Bajura & Szewczyk (1970) for flow along a plane surface and by Newman (1961) for flow along a cylindrical surface. Bajura & Szewczyk determined that transition occurred for distance Reynolds numbers of order 2×10^5, while Newman observed laminar flow at distance Reynolds numbers to only 3×10^4. The larger transition Reynolds numbers (2×10^5) observed by Bajura & Szewczyk may be attributable to careful control of the upstream conditions, and the ambient environment near the test section. Momentum integral techniques were successfully applied by Reddy Gorla & Jeng (1972), to predict the characteristics of a laminar plane wall jet emerging from a long, narrow slit. Their numerical results were in good agreement with the experimental data of Bajura & Szewczyk, when correlated in terms of the exit Reynolds number.

The stability characteristics of the plane wall jet were computed by Chun & Schwarz (1967), for the case of temporally growing disturbances. The critical Reynolds number was determined to be 57. Disturbances in the outer region, near the location of the point of inflexion in the velocity profile, exhibited the greatest growth of the three-amplitude maxima obtained from the solution for the streamwise velocity component. The other two-amplitude maxima occur in the inner region, where the mean velocity is about half the maximum velocity, and in the outer region, where the mean velocity is essentially zero. The experimental observations of Bajura & Szewczyk are in good agreement with these predictions of linear theory. It must be recognized, however, that spatially growing disturbances are observed in the laboratory, in contrast to the temporally growing disturbances predicted by the solutions of Chun & Schwarz. Except for the curves of neutral stability, Gaster (1965) has shown that significant errors can occur in comparing results obtained by these two methods, if the wave speed varies with wavenumber.

2.2. *Transition in shear layers and free jets*

2.2.1. *Shear layers.* Free shear layers may be formed by the merging of two streams, which are initially separated by a thin plate, or by flow over a rearward facing step. If the upstream flow is maintained below the critical Reynolds number for the initiation of transition in the wall boundary layer, the free shear layer develops smoothly, and suffers little memory effect from the upstream boundary layer. In studies of separated shear layers (Sato 1956, 1959; Browand 1966), the growth of small sinusoidal disturbances was observed downstream from the step. In these initial stages of transition, the flow was two-dimensional. Browand demonstrated that the initial nonlinear distortion of the instability wave was first made manifest by the growth of a subharmonic component, which occurred without significant distortion in the spanwise direction.

The reason for the occurrence of the subharmonic component in the hot-wire signals of Browand is illustrated in the smoke pictures taken by Freymuth (1966) in a free jet. The boundary layers along the interior of the nozzle were thin compared with the nozzle diameter, so that opposite regions of the shear layer did not interact. Freymuth identified the process of transition as occurring in four zones: namely, (i) a transformation region from a wall boundary layer to a free shear layer; (ii) a region of linear (exponential) growth of disturbances; (iii) a nonlinear region of growth, wherein discrete vortices were formed; and (iv) a region of turbulent flow. In the nonlinear region, the smoke filaments began to roll up into discrete vortices, and later rotated around each other. This rotation was the result of the outward migration of a vortex into a lower velocity region, and the associated motion of its trailing vortex into a higher velocity region. This combined vortex system then rotated in the same direction as the initial vortices. The spacing between vortex pairs was twice the initial spacing before pairing. Therefore, a halving of the frequency is obtained, as was reported by Browand. This mechanism was clearly demonstrated in the work of Winant & Browand (1974), for a free shear layer formed by the merging of two parallel streams. The formation of discrete vortices led to pairings of the type shown by Freymuth; however, repeated pairings of the doubled vortices were observed as the flow proceeded downstream. The motion of the vortices in rolling around each other was essentially two-dimensional.

2.2.2. *Plane free jets.* Transition in plane free jets was studied by Sato (1960), Sato & Sakao (1964), Beavers & Wilson (1970) and Rockwell & Niccolls (1972), who identified four zones in the transition process similar to the regions noted by Freymuth. The rolling up of the flow into discrete vortices was followed by two different types of coalescence between adjacent vortices, which Rockwell & Niccolls called *mature-stage coalescence* and *nascent-stage coalescence.* Nascent coalescence occurred when the vortices were in an immature stage of development. In the nascent stage, the embryonic vortices appeared to stagnate and slide into one another, with a folding but no net rotation of the vortex system, as described by Winant & Browand. A cascading effect, where the mature-stage coalescence resulted from a pairing of vortices that previously experienced nascent-stage coalescence, was also observed in some of the transitions. The

mature-stage coalescence process brought about a rapid widening of the jet, whereas nascent coalescence did not greatly disturb the mean flow.

These observations both in the free jet and in shear layers show the two-dimensional nature of the breakdown process, and identify the mechanism of vortex pairing as the initial nonlinear motion in the transition to turbulent flow. The introduction of acoustic disturbances at frequencies corresponding to the most amplified frequency band for the shear layer was shown to control the transition process by fixing the transition location. Similar results were observed when the hot-wire signal was fed back into the flow acoustically.

2.3. *Transition along flat plates*

In comparison with the two-dimensional, inviscid type of transition characteristic of shear layers and jets, Klebanoff, Tidstrom & Sargent (1962) have shown that transition along a flat plate is strongly three-dimensional in the nonlinear stages of growth of the disturbance. The initial appearance of small-amplitude perturbations of the mean flow is two-dimensional, but this initial wave develops a three-dimensional pattern, which results in portions of the vortex line associated with the disturbance being convected upward into regions of higher mean velocity. The vortex-line segment in the faster-moving regions is transported downstream ahead of the slower-moving segments. As a result of the stretching of the vortex line, the velocity fluctuations associated with the disturbance are intensified. The eventual breakdown of the vortex line is due to a secondary instability associated with the kink in the velocity profile identified by the hot-wire studies of Kovasznay, Komoda & Vasudeva (1962).

Visual observations of the transition process have been reported by Fales (1955), Hama, Long & Hegarty (1957), Hama (1960) and Hama & Nutant (1963) on flat plates, and by Knapp & Roache (1968) for ogive nose cylinders aligned parallel with the flow. The smoke pictures of Knapp & Roache led to the identification of five regions in the transition process: (i) the formation of a set of two-dimensional Tollmien–Schlichting waves; (ii) a region of three-dimensional deformation of these waves; (iii) a pattern of vortex trusses (the stretched vortex lines described above); (iv) the breakdown of the vortex trusses into turbulence; and (v) a region of re-laminarization following the breakdown. (The re-laminarization, or downstream intermittency effect, is absent in free shear layer flows.) Re-laminarization was attributed by Brown (1965) to the establishment of a local favourable pressure gradient immediately following the breakdown. The breakdowns occur in sets separated by laminar regions for natural transition. Forcing of the boundary layer by acoustic disturbances resulted in the disappearance of the downstream intermittency. Knapp & Roache concluded that breakdown under conditions of forcing occurred as individual vortices, instead of the sets observed in natural transition.

The main conclusion from the visual and hot-wire studies is that a three-dimensional deformation of the disturbance pattern is an integral part of the transition process. The streamwise distances travelled by the flow during the

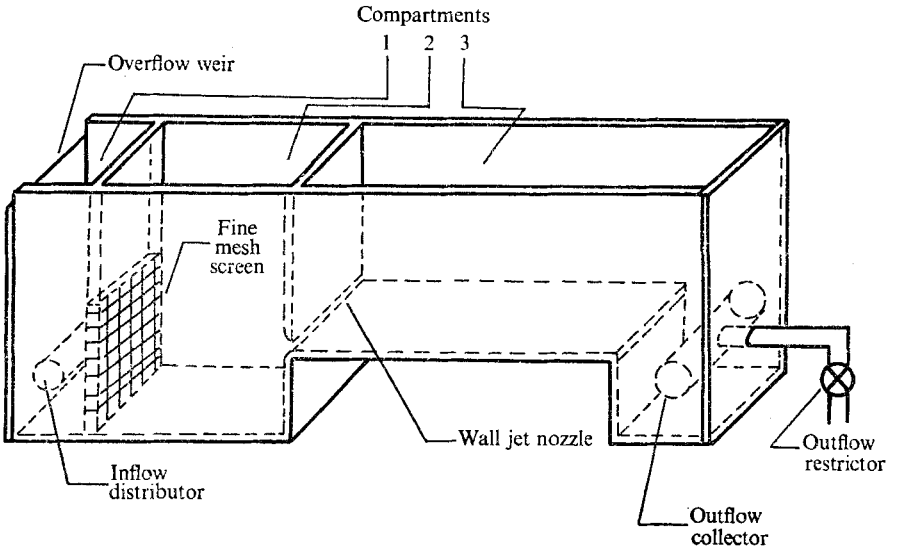

FIGURE 1. Pictorial view of wall jet test facility. Overall dimensions: length 107 cm, height 46 cm, width 30 cm.

different stages of transition are large compared with the boundary-layer thickness. Streamwise distances for transition in wall-boundary-layer flows are much larger than those for transition in free shear layers.

3. Description of wall jet test facility

3.1. *Experimental facility and instrumentation*

The experimental facility, illustrated by figure 1, was constructed from 1·270 cm thick clear Plexiglas. Water from an elevated reservoir entered compartment 1 through the inflow distributor. A narrow slit of height $L = 0{\cdot}0635$ cm allowed water to flow from compartment 2 into compartment 3, to produce the wall jet. Different exit speeds were obtained by regulation of the outflow restriction, to attain a given water level difference between compartments 2 and 3. The water tunnel was designed with a free surface in all three compartments, to minimize extraneous disturbances from the water supply system and vibrations from the structural supports. All water flows were returned to a large sump, and continually recirculated with the fluid in the elevated reservoir. Temperature measurements obtained during data taking experiments indicated differences of no more than 1 °C from top to bottom in the test facility, with most of the variation in temperature occurring in a thin layer near the free surface. The overall dimensions of the experimental facility were approximately $107 \times 46 \times 30$ cm. The test section was 30×61 cm^2 in surface area, and had water to a nominal depth of 25 cm for experimental investigations. The maximum vertical extent of the laminar wall jet flow field varied from 1 to 3 cm, depending on the exit Reynolds number.

Two exit nozzle configurations, called *jet nozzle* and *channel nozzle*, were

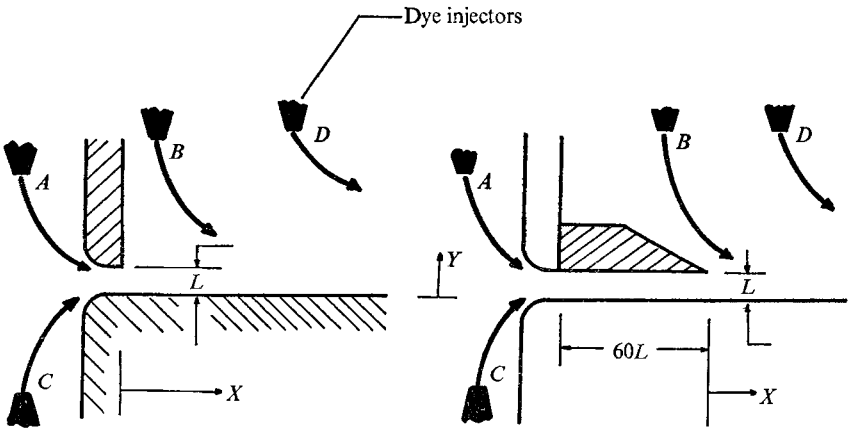

FIGURE 2. Sketch of nozzle configurations.

Injector	Location	Purpose
A	Plenum chamber near upper edge of nozzle	To mark dividing zone between inner and outer regions
B	Approximately 40 slit heights downstream from exit and 80 slit heights above plate surface	To entrain dye into outer region from ambient
C	Plenum chamber near lower edge of nozzle	To mark fluid in inner region
D	Approximately 120 slit heights downstream from exit and 160 slit heights above plate surface	To show penetration of detached wall jet into ambient fluid

TABLE 1. Dye injector locations

used during the experiments. The jet nozzle illustrated by figure 2(*a*) was fabricated by matching a 0·953 cm radius on the edges of two 1·270 cm thick sheets of Plexiglas, to produce the curved portions of the nozzle. The remaining portion of these Plexiglas sheets formed a parallel channel, with a length–height ratio of 5 at the exit of the nozzle. The transverse dimension of the jet nozzle was 30 cm, the spanwise dimension of the test section. Figure 2(*a*) illustrates four sets of streaklines, corresponding to the path followed by dye injected from various locations near the nozzle. The injectors are denoted by the symbols *A*–*D*, and are described in table 1. The channel-nozzle configuration, shown by figure 2(*b*), was formed by the addition of a wedge section to the original jet nozzle. The spanwise extent of the nozzle was also reduced to a width of 10·2 cm, centrally located along the centre-line of the test section. The wedge insert was machined with a 34° backwards slope. The length–height ratio of the channel nozzle was 60.

Flow-visualization experiments were performed using dye injectors and hydro-

gen-bubble generators. Photographic results were obtained with a Hycam high-speed camera, equipped with a half-frame 16 mm lens system, and also with a single-lens-reflex 35 mm camera. The 16 mm film was studied on a time-motion analyser. Hot-film probes (Disa S & B) were used, to obtain mean and fluctuating streamwise velocity components. Frequency spectra were obtained from the hot-film signals, on a Bruel & Kjaer frequency analyser. Disturbances were introduced into the flow field during forced-transition experiments by a loud-speaker resting on top of the test section.

3.2. *Calibration*

3.2.1 *Jet nozzle.* Time-streaklines, generated by the hydrogen-bubble technique, showed that the flat-plate surface within 12 cm on either side of the centre-line of the test section was a two-dimensional flow region for distances of interest in the downstream direction. These observations were confirmed by studies of streaklines, which emerged from a wide-mouth dye injector (0·3 cm × 10 cm), and also by measurements taken with a hot-film probe. The volume flow rate through the nozzle was measured by weighing the efflux from the outflow collector for a fixed time period under steady flow conditions. The flow from the nozzle was also used to calibrate the linearized hot-film probes (Catalano 1971).

3.2.2. *Channel nozzle.* For the channel nozzle, the exit velocity profile is parabolic, and the maximum velocity is 1·5 times the average velocity (Schlichting 1960). Visual observations of dye streaks from the wide-mouth injector indicated that the flow from the channel nozzle remained two-dimensional for at least 240 slit heights downstream from the exit, for at least 3 cm on either side of the centre-line of the test section. Hot-film probe investigations were not performed with the channel nozzle, since the exit velocity profile was similar to that of Bajura & Szewczyk, and close agreement with their previous results was observed for the more dissimilar jet nozzle design.

3.3. *Transition lengths*

The first set of experiments was conducted with the jet nozzle configuration. The transition length was quite variable from day to day, and the flow was sensitive to disturbances. The channel nozzle was later designed with the hope of reducing the intense shear zone in the outer region immediately downstream from the exit. These efforts were successful in extending the transition length to, say, 160 slit heights downstream for cases where the jet nozzle would produce laminar flows to only 80 slit heights downstream. In general, transition distances with either nozzle were much shorter than those observed by Bajura & Szewczyk. The most stable conditions in the present experiments were obtained when the general activity level in the entire laboratory was at a minimum.

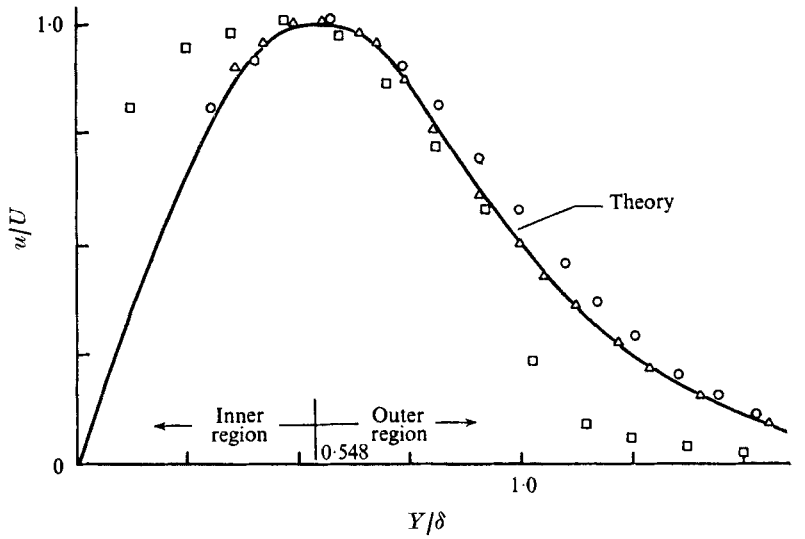

FIGURE 3. Normalized velocity u/U plotted against the dimensionless vertical distance Y/δ. Exit Reynolds number is 445. □, $X=L$; ○, $X=10L$; △, $X=20L$.

4. Hot-film anemometry studies with jet nozzle configuration

The reference quantities used in defining the exit Reynolds number R_e are the maximum exit velocity V_e and the slit height L. Experimental observations were limited to flows in the Reynolds number range 100–600. Detailed investigations of flows, with exit Reynolds numbers of 103, 275 and 445, were also documented on high-speed 16 mm colour film (Catalano 1971).

4.1. *Laminar flow region*

The development of the laminar plane wall jet velocity profile is shown for an exit Reynolds number of 445 in figure 3. The data are normalized with respect to the local maximum velocity U and the local boundary-layer thickness δ (which is defined as the distance from the wall to the point in the outer region where the velocity is one half the local maximum velocity). The agreement with the theoretical velocity profile (solid curve) is good. The local maximum velocity was found to decrease with downstream distance to the $\frac{1}{2}$ power and the boundary-layer thickness increased with distance to the $\frac{3}{4}$ power, in agreement with the predictions of Tetervin & Glauert. The virtual origin was in agreement with the previous data of Bajura & Szewczyk. Since the data for the mean flow field could be closely predicted by the correlations developed by Bajura & Szewczyk, their results were used to calculate the characteristics of the mean flow field in terms of the exit Reynolds number for subsequent experiments with both the jet- and channel-nozzle configurations.

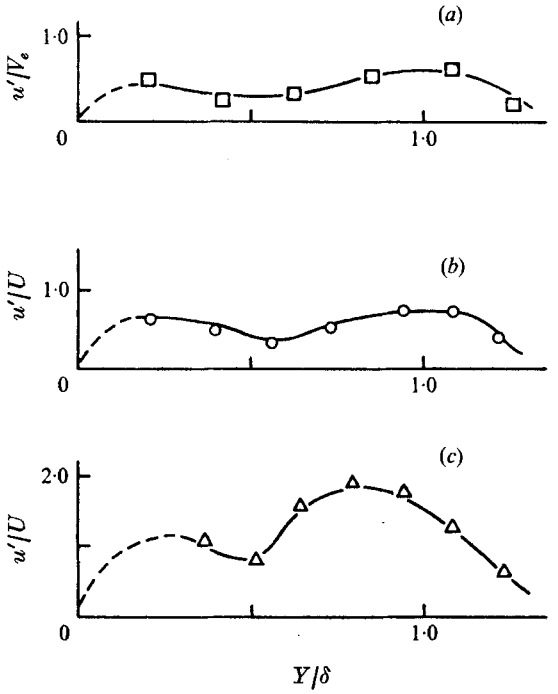

FIGURE 4. Relative amplitude of the streamwise velocity component u', in per cent, plotted against the dimensionless vertical distance Y/δ, at three downstream stations. Exit Reynolds number is 445. (*a*) $X = L$; (*b*) $X = 10L$; (*c*) $X = 20L$.

4.2. *Initial stages of transition*

The length of the combined laminar–transition range varied from 40 to 120 slit heights for the jet nozzle, the longer distances being associated with the lower exit Reynolds numbers and low levels of background disturbances. The distribution of the fluctuating velocity component u' at several downstream stations is shown in figure 4. At $x = 20L$, the larger amplitude maximum occurs in the outer region, near the point of inflexion in the velocity profile ($Y/\delta = 0{\cdot}88$). A relative minimum occurs near $Y/\delta = 0{\cdot}548$, the point of maximum velocity. The smaller amplitude maximum in the inner region occurs near $Y/\delta = 0{\cdot}20$, where the velocity is about $0{\cdot}5U$. This disturbance behaviour is similar to the theoretical predictions of Chun & Schwarz (1967) and the experimental observations of Bajura & Szewczyk.

In accordance with the assumptions of linear stability theory, the initial disturbance field should be organized with a characteristic frequency, denoted here by the symbol f_p. Frequency spectra near the exit were relatively flat. A disturbance of a well-defined frequency was present at $X = 10L$. At the station $X = 20L$, the spectrum shown by figure 5 was obtained. The small peak at 175 Hz corresponds to the eddy shedding frequency of the hot-film probe. The large peak at 50 Hz corresponds to the characteristic disturbance frequency f_p, for the initial (linear growth) stages of transition. The additional peak near 28 Hz is

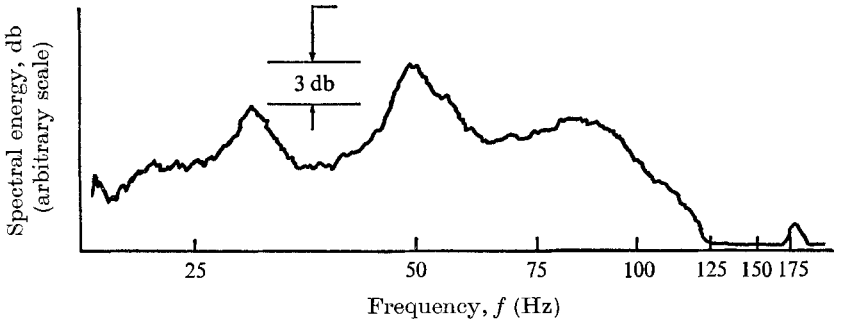

FIGURE 5. Energy spectrum of the disturbance velocity component u', at $X = 20L$ and $Y/\delta = 0{\cdot}85$ for an exit Reynolds number of 445.

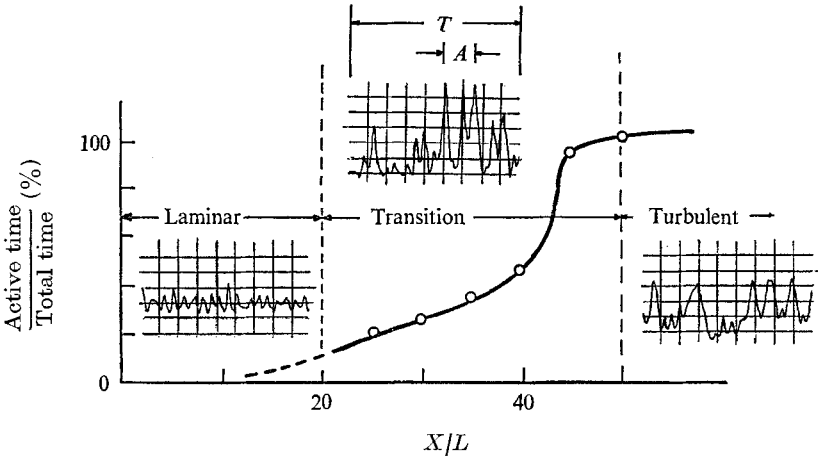

FIGURE 6. Downstream intermittency plotted against the dimensionless downstream distance X/L for an exit Reynolds number of 445.

approximately one half the frequency of the primary disturbance. This spectrum indicates that the wall jet is no longer in the linear stability regime, although the disturbance intensity is barely 2 % of the local maximum velocity. In the initial stages of transition, the signals appeared periodic, and the number of zero crossings correlated well with the primary frequency of the disturbance, as obtained from the frequency analyser. The hot-film signals were also seen to 'lock in' and become amplified when the wall jet flow was excited by sinusoidal acoustic signals of the same frequency range. These forced disturbances were generated by a loudspeaker in physical contact with the test section, and were transmitted to the flow primarily by the structural vibrations induced in the test facility. It was observed that, when the loudspeaker was not in physical contact with the test facility, the locking-in effect could not be attained, even at greatly increased acoustic power levels. By forcing the flow with the acoustic signals, the transition distances were seen to decrease, and the level of activity of the disturbances was seen to increase at a given downstream station. Similar results were obtained when the amplified signal from the hot-film probe was fed back acoustically into the test section.

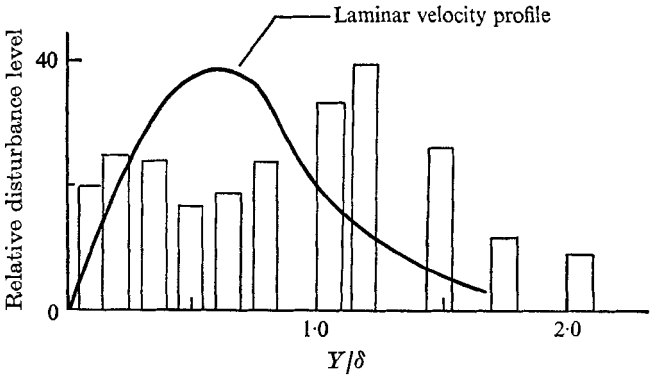

FIGURE 7. Vertical activity distribution at $X = 25L$ for an exit Reynolds number of 445.

4.3. *More advanced stages of transition*

Further examination of the hot-film probe signals revealed occasional voltage spikes, which indicated rapid excursions of the fluctuating velocity component u' toward higher velocity levels. A downstream intermittency function for the transition process was defined as the ratio of the time (length of record on strip chart recorder) for which the activity denoted by the higher velocity spikes appeared divided by the total time (total length of record). This intermittency function is illustrated on figure 6 for an exit Reynolds number of 445. The fully-turbulent regime was arbitrarily defined as the condition for which the entire record consisted of only large-amplitude, random frequency oscillations. No attempt was made to determine if the velocity profile at these stations was that of a fully-developed turbulent wall jet. Figure 6 shows that the transition process for the jet-nozzle configuration occurred in the rather short distance of about 20 slit heights (equivalent to 13 local boundary-layer thicknesses) for this exit Reynolds number.

The vertical location of these intense regions of activity, at a given downstream station, is illustrated by figure 7. The number of voltage spikes occurring at each level was counted for a fixed time period. The histogram formed by the data is similar to the amplitude distribution of the disturbance velocity component u' given by figure 4. (Note that the data record does not cover the entire range of Y/δ and, therefore, the absence of a data point does not imply that no disturbances are present.) In contrast with figure 4, however, the activity in the outer region has been displaced further from the wall into a region of lower velocity. The level of activity in the inner region remains high, but at only one half the level of the outer region disturbances. Near the point of maximum velocity, the number of voltage spikes observed is somewhat depressed compared with the inner and outer regions. The fluid motions in both the inner and outer regions appear to be confined to each region separately and no interaction between regions was occurring (i.e. on the average) at this downstream station. Hence the maximum velocity sector of the profile is acting as a dividing area between the inner region wall boundary layer and the outer region shear layer. This observation was verified by analysis of high-speed films of the initial stages of transition.

5. Visual observations of natural transition

5.1. *Introductory comments*

Visual observations of the transition process for the jet-nozzle configuration were made concurrently with the hot-film probe investigations. Dye was introduced into the wall jet flow primarily from the two injectors A and C, located in the settling chamber. The injected dye streams were released from flattened tubes, which initially had a nominal diameter of 0·30 cm. The injectors were adjusted, so that the dye flowed very slowly into the settling chamber, at a distance of at least 3 cm from the entrance to the nozzle. Both the dye-coloured water and the clear water then passed through the contraction section of the nozzle (40 to 1 contraction ratio) and into the test section.

One dye injector C was located so that the emerging wall jet flow would be marked with dye in the inner region, near the location where the velocity was one half the maximum velocity. This region corresponds to the disturbance centred at $Y = 0{\cdot}2\delta$, as shown in figure 4. The other injector A was adjusted to allow the dye to flow as close as possible to the upper edge of the exit nozzle. It was expected (Bajura 1967) that the streamlines marked by this dye streak would be in the outer region activity zone near $Y = 0{\cdot}8\delta$. However, the photographic and hot-film probe data indicated that this dye streak more nearly followed a path coincident with the locus of points of maximum velocity. This result was obtained with both the jet- and channel-nozzle configurations.

In view of the rather limited transition range available for investigation with the jet nozzle, the alternative channel-nozzle design was introduced for further visual and photographic examination of the transition process. The sensitivity of the wall jet flow from the channel nozzle was similar to that of the jet-nozzle design, with respect to the introduction of forced disturbances. The advantage obtained from the channel-nozzle design, however, was that natural transition was postponed to much larger downstream distances. As a result, it can be stated that the natural transition process observed with the channel nozzle was not unduly influenced by the conditions at the exit from the nozzle nor the nozzle design. Hence, the growth of disturbances predicted by linear stability theory began somewhere in the downstream range of the wall jet flow rather than in the nozzle itself. Photographic data for the channel-nozzle experiments were obtained only during the evenings of weekends or holidays, when the largest transition distances could be attained. Experiments conducted with different dye injection rates and locations showed that the method of injection was not responsible for the early transition observed for the wall jet flow from either nozzle.

5.2. *General description of natural transition at moderate Reynolds numbers*

High-speed motion-picture films were taken of the transition process for both the channel- and jet-nozzle configurations. The overall mechanism of transition was observed to be the same for both nozzles. The process of natural transition, as studied with the channel-nozzle configuration, will be described first. These

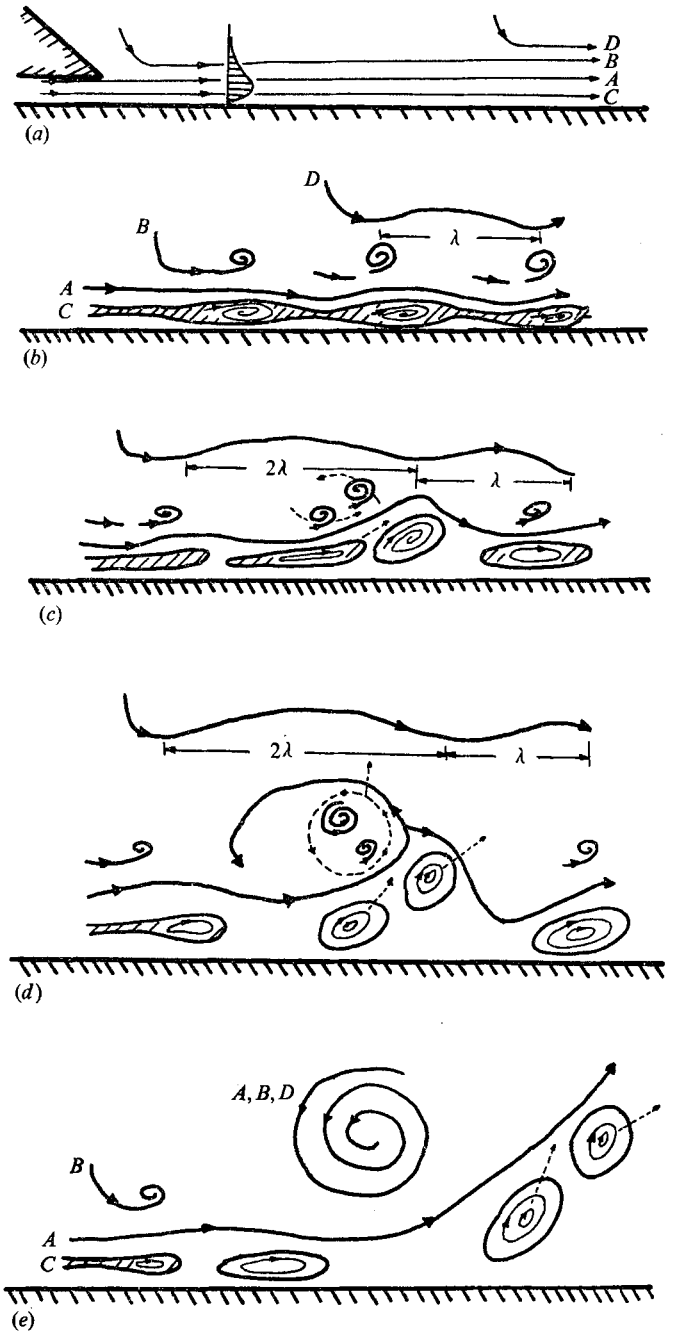

FIGURE 8. Illustration of the behaviour of dye streaks during various stages of transition at moderate Reynolds numbers.

comments apply to wall jets with exit Reynolds numbers in the range 200–600. Figure 8(*a*) illustrates a laminar velocity profile with the flow direction oriented from left to right. Also shown are representative streaklines from the various dye injectors. Fluid in the inner region has a clockwise vorticity (CW) and fluid in the outer region has a counter-clockwise vorticity (CCW) under steady flow conditions. Sequences (*b*)–(*e*) of figure 8 illustrate the stages of breakdown from laminar to turbulent flow, for situations where transition initiates downstream from the exit nozzle.

Transition generally occurred in the following stages: (i) the formation of discrete vortices in the outer region; (ii) the pairing of two or more vortices in the outer region, coupled with the possible pairing of vortex-like motions in the inner-region wall boundary layer; (iii) a lifting-off of the wall jet flow into the ambient fluid; (iv) dispersion of the lifted-off flow field by three-dimensional turbulent motions; and (v) re-laminarization of the upstream flow, until another vortex pairing occurred.

5.3. *Detailed description of the stages of transition*

Figures 8–10 illustrate the natural transition process, and will be discussed simultaneously. The thickness of the boundary layer is much less than the streamwise distance over which transition occurs. Therefore, the viewing region for observations is long and narrow. Since transition activity is not fixed to a given location, close-up pictures which contain sufficient upstream and downstream history to trace the motions of the dye streaks were difficult to obtain. The original photographs of figure 9 were in colour, and showed more detail than is possible in the present black-and-white.

5.3.1. *Stage one: formation of discrete vortices.* The outer region dominated the transition process. Figure 8(*b*) shows that the growth of small disturbances is more rapid in the outer region. Discrete vortices develop first in this region. A photograph showing the initial concentration of dye into discrete patches is shown by figure 9(*a*) (plate 1). Dye is being introduced from injectors *A* and *B* only. Neither dye streak is in the region of intense CCW rotation; and the dye pattern marks the outer fringes of the disturbance activity. Motion of dye streaks in the inner region (not illustrated in figure 9(*a*)) is indicated in figure 8(*b*) as a tendency for the inner dye stream to form an identifiable region of dyed fluid, having a tendency to rotate in the CW direction. The disturbance activity in the inner region in the first stage of transition is not as intense as in the outer region, and is manifested as a bulging of the dye streaks. The bulges are separated uniformly from each other, in a matched correspondence with disturbances in the outer region. The inner-region bulges tend to be slightly ahead of the outer-region disturbances as the pattern travels downstream.

5.3.2. *Stage two: vortex pairing.* Figure 8(*c*) illustrates the tendency for two consecutive vortices in the outer region to begin to rotate around each other and form a doubled vortex, or vortex pair, which rotates as a whole in the same CCW direction. The individual vortices also continue to rotate in the CCW direction. The induction process may originate from several sources. The most common observation, shown by figure 8(*c*), involves the intensification of the

leading vortex into a larger rotating mass of fluid, such that the trailing vortex is induced to join in the rotation. During this intensification process, the leading vortex appears to be retarded in its downstream travel, and rises into a lower velocity region.

The other type of pairing process in the outer region involves minor disturbances, which appear to be of equal strength, such that neither appears dominant. Such an occurrence is illustrated by figure 9 (*b*) (plate 1). The photograph shows that the pairing is occurring approximately midway between the disturbances. The dye patch (1*a*) has risen to a position above the plate where the mean velocity is less than the velocity where it originated. Dye patch (1*b*) has moved to a higher velocity region, as indicated by its lower position compared with the other streak markers that issued from injector *B*. Note that the streakline from injector *A* is undisturbed by this pairing process, unlike the motions shown by figure 8 (*c*).

In view of these two slightly different pairing mechanisms, it is postulated that the relative strengths of the two vortices involved in the pairing process may depend on the manner in which the disturbance was introduced into the flow field, or on the random spacing between vortices which occurs in a natural-transition. The vortex pairing illustrated by figure 8 (*c*) may be termed a *mature-stage coalescence* (after Rockwell & Niccolls 1972). The pairing shown by figure 9 (*b*) may be termed a *nascent-stage coalescence*. Nascent-stage coalescence is very weak; and the dye patches may merely be indicators of embryonic vortices, which have not had sufficient time to develop into an identifiable vortex pattern. In agreement with the results of Rockwell & Niccolls, mature-stage coalescence brings about a marked broadening of the flow field (figure 8 (*c*)), whereas the nascent-stage coalescence does not (figure 9 (*b*)). It is possible that the disturbances which underwent nascent-stage coalescence will undergo a later mature-stage coalescence, as described by Rockwell & Niccolls and as observed by Winant & Browand (1974). The wavelength of the pairing process is approximately twice the separation distance of the unpaired vortices, as illustrated by figure 8 (*c*). The doubling of the wavelength corresponds to the halving of the frequency f_p, illustrated by figure 5.

The behaviour of the inner region during this second stage of transition is dependent on the above two types of pairing mechanisms. When the pairing process is dominated by the leading vortex (figure 8 (*c*)), the motion in the inner region is such that the embryonic inner vortex, which corresponds to the leading vortex of the outer region, also intensifies. This inner vortex then begins to rise from the surface of the plate, and displaces upwards the dye streak *A*, marking the maximum velocity region. The trailing embryonic vortex in the inner region also begins to intensify, and advance in response to the forces induced by the other rotation field. The two vortices in the inner region begin to emerge as discrete regions of rotation, with no connecting dye streaks between them, as the pairing process in the outer region continues. This behaviour is illustrated by the displacement of dye streak *A* in figure 9 (*c*) (plate 1), which occurs as a result of the growth of the leading vortex in the inner region. (The arrow (2*a*) denotes the apparent location of this inner-region vortex.)

Figure 9 (*d*) (plate 2) illustrates the transition process for a case when all four

dye injectors are used to mark the flow. The arrow (1*a*) denotes a discrete vortex in the outer region, which is downstream of the transition area denoted by vortex (1*b*). This behaviour indicates that the transition is occurring naturally owing to random disturbances; otherwise, a region of non-turbulent flow would not exist downstream of region (1*b*). Note that the corresponding inner-region vortex (2*a*) is now a discrete rotating region, as opposed to the more continuous dye streaks observed near the nozzle. The dye streak between vortices (1*a*) and (2*a*) originated from injector *A*, and still serves as a dividing zone between the inner and outer region, despite the large-amplitude disturbance activity on opposite sides of the dye streak. This observation supports the previous conclusion that the inner and outer regions are not interacting during the initial stages of transition.

The terminus of the arrow for vortex (1*b*) denotes the vortex pair which originated the transition process. This fluid was distinguished on the colour film as having originated from injector *B*. The larger rotating core surrounding vortex (1*b*) is comprised of fluid that emerged from injector *A* behind the nozzle and travelled downstream near the region of maximum velocity. Vortex (2*b*) is an inner-region vortex, whose growth has aided in lifting the wall jet off the plate. The trailing inner-region vortex is being induced to follow off the plate, although this trailing vortex has not yet intensified sufficiently to assume the customarily imagined circular shape.

Figure 8(*d*) illustrates a case where the two vortices in the inner region also coalesce. This type of behaviour occurs when the inner-region vortices become well defined before vortex pairing occurs in the outer region. An inner-region pairing occurs when the trailing vortex rises into a higher-velocity region, and overtakes the leading vortex by encircling it from above. The combined vortex system then rotates with a CW motion, while the individual vortices also continue to rotate in the same direction. The general motion of the combined vortex system is upwards into the ambient fluid, with a drift in the downstream direction. Inner-region pairings were very infrequent.

5.3.3. *Stage three*: *lift-off*. Figures 8(*d*) and (*e*) illustrate the initial and final stages, respectively, of a process which results in the wall jet flow leaving the surface of the plate, and penetrating deeply into the ambient fluid. The large rotating zone shown in figure 8(*d*) continues to draw outer-region fluid into the rotating pattern. The dye streak from injector *A* is initially disturbed by the roll-up and lift-off process (figure 8(*d*)), but later resumes its previous role as a dividing zone between the inner and outer regions (figure 8(*e*)). The vortex pattern in the inner region travels into the ambient fluid at a position slightly below streakline *A*. These inner-region vortices continue their clockwise rotation, and may at a later time coalesce, owing to mutual induction, and rotate around each other in a clockwise motion.

A photograph of the later stages of lift-off is shown by figure 9(*e*) (plate 2). The region marked (1) contains rolled-up patches of fluid from the outer region, along with some of the fluid from injector *A* that was initially trapped into the rotating pattern. The vortices (2*a*) and (2*b*) in figure 9(*e*) are inner-region vortices that have lifted off the surface of the plate.

During the final stages of the lift-off process, the inner-region dye patches will continue to roll up and leave the surface continuously, in the same manner as the initial vortices. Fluid upstream from the lift-off point continues to feed into the rotating zone. The motion in the outer region becomes stabilized to a certain extent after the lift-off. Since the initial outer-region vortex has rotated in a wide arc into the ambient fluid, it subsequently induces a slow motion upstream of the lift-off location, such that the ambient fluid near the fringes of the wall jet boundary layer has a drift velocity in the direction of the mean flow. This condition may create a favourable situation for increasing the stability of the flow, by reducing the effective shearing velocity between the wall jet outer layer and the ambient fluid. The flow upstream of the lift-off point will then re-laminarize for a brief period, until another outer-region vortex doubling occurs that is strong enough to cause a lift-off of the type described here.

In the natural transition case, the activity of doubling was seldom seen to occur as an isolated action. Usually the dye pattern would become disturbed in sets of several eddies. The eventual breakdown would then occur, as illustrated by figure 9(*d*), where the lift-off point is at the end of a string of rather large amplitude disturbances, such as the vortices (1*a*) and (2*a*). The pattern of breaking down in sets separated by laminar-like regions is similar to the process described by Knapp & Roache for transition in a wall boundary layer.

5.3.4. *Dispersion of dye streaks.* As the penetration of the lifted-off flow continues into the ambient region, the dye streaks become dispersed by motions that are distinctly three-dimensional. A wavelike structure in the spanwise direction was occasionally observed during experiments with the jet-nozzle configuration, at the beginning of the dispersion sequence, when the flow was viewed from directly overhead. Attempts to correlate the spanwise wavelength with a characteristic length of the flow field, like the boundary-layer thickness, yielded inconclusive results. Data for exit Reynolds numbers of 445, 275 and 103, taken with the jet-nozzle configuration, indicated that the spanwise wavelength during the initial portions of this three-dimensional deformation stage was constant at a value of 16 times the slit height of the exit nozzle. It could not be determined if this condition was inherent to the flow breakdown, or a function of conditions in the upstream plenum. The dye streaks broke down into random turbulent motions soon after formation of the three-dimensional pattern. In many instances, breakdown occurred without any indication of a spanwise periodicity. Detailed observations of this stage of transition were difficult, owing to the dispersive action of the dye streaks, and inability to examine both the overhead and side views of the flow field simultaneously. When flow from the channel nozzle was viewed from overhead, no identifiable spanwise wavelength was observed. Since the channel-nozzle design was less sensitive to extraneous disturbances to the entrainment shear layer at the exit, the absence of an identifiable spanwise pattern supports the conclusion that wall jet transition is essentially two-dimensional.

The turbulent mixing process results in the distribution of inner-region fluid far into the ambient, and brings outer-region fluid near the surface of the plate. Dispersion activity was observed at heights from 4 to 8 cm off the plate. The

extent of the flow field above the plate surface is much broader for the turbulent flow than for the relatively narrow laminar boundary layer. These dispersive motions are shown on the downstream edges of figures 9(*d*) and (*e*) (plate 2).

5.3.5. *Re-laminarization.* A period of re-laminarization of the mean flow field follows the breakdown process, as described in §5.3.3. The length of time (or separation) between breakdowns depended on the Reynolds number, the breakdown location and the general disturbance level in the ambient fluid. If a reference time for the flow is defined in terms of the slit height and the maximum nozzle exit speed (i.e. $T_r = L/V_e$), then a dimensionless time between lift-offs can be defined as $t^* = t/T_r$. The dimensionless time between lift-offs has been observed to be as great as 2000 or larger. Dimensionless times corresponding to the primary frequency of the disturbance were in the neighbourhood of 50. The large value of t^* for the re-laminarization process indicates the influence of the recirculation zone in the outer region in controlling the behaviour of the fluid upstream from the lift-off point.

5.4. *Two-dimensionality of natural transition*

Figure 10 (plate 3) illustrates a transition boundary layer as seen from behind and slightly above the channel-nozzle exit. The dye flow was introduced from behind the nozzle at locations *A* and *C*. Injector *C* in this experiment had an exit of dimensions 7·5 × 0·3 cm. Dye from this injector emerged from the nozzle as a sheet and travelled downstream in the inner region. Two 0·3 cm diameter dye injectors were used at locations *A* and were separately positioned on opposite ends of injector *C*. Fluid from these latter two injectors travelled in the outer region, near the edges of the sheet of dye marking the inner region. The two dye streaks from injectors *A* appear as the darker bands in figure 10.

The two-dimensional nature of the initial stages of transition is illustrated by the dark region, denoted by (*a*), in figure 10. This line corresponds to the rolling-up of the inner region, and is relatively undistorted in the spanwise direction. The corresponding dye streaks in the outer region are in similar stages of transition, despite the fact that they are separated by a distance of about 30 boundary-layer thicknesses. Further downstream from location (*a*), where transition is further advanced, the activity in the outer region is not as strongly co-ordinated in the spanwise direction, as shown by location (*b*). The near dye streak is in a state of rotation in the outer region, while the corresponding streak on the opposite side of the test section is only initiating this type of activity. Region (*a*) illustrates the initiation of a new independent transition, while region (*b*) appears to be strongly influenced by the three-dimensional activity further downstream. Once the lift-off process has been completed, the dye streaks exhibit a sinuous, three-dimensional motion, as shown on the extreme downstream edge of figure 10.

The term 'two-dimensional' should be qualified in this respect. The ratio of the spanwise length of a vortex filament (i.e. the distance across the flow field) to the local boundary-layer thickness, during transition, was as large as 50:1 for the channel-nozzle experiments in the linear range of transition at down-

stream distances of 200 times the width of the exit nozzle. Some natural variation in even the most rigorous two-dimensional exit flow conditions can be expected over this range. Hence, some waviness could be expected in the spanwise direction for natural transition, in contrast to the rigidly two-dimensional transitions observed when forcing was applied.

When transition is induced by the intensification of the leading vortex in the outer region, simultaneous activity occurs across the entire span of the test section. This type of transition can be initiated by an organized disturbance, such as acoustic excitation or a sudden jarring of the test facility. In these cases, the entire lift-off process is two-dimensional and, occurs much farther upstream than the natural transition illustrated by figure 10. However, if no organized stimuli are introduced, then natural transition can occur, owing to the growth of a small random disturbance, which is not organized, over large spanwise distances. Natural disturbances may arise owing to minor variations in the velocity or dimensions of the exit nozzle, or random recirculation currents in the test facility. In this case, the movement of local vortices into higher- or lower-velocity regions can cause three-dimensional variations in the flow field, and vortex line stretching by the faster moving fluid would result. Transitions, that featured a vortex line stretching mechanism in the initial stages, could not be clearly identified. In instances where vortex line stretching might have occurred, only a few boundary-layer thicknesses in the downstream direction separated the initiation of the breakdown at one spanwise location from a corresponding motion at another spanwise location, at roughly the same downstream distance from the nozzle exit. Because of the highly unstable nature of the outer region, a vortex line stretching mechanism, if present, could not remain inactive for great distances downstream. No bursts, or turbulent spots, common to wall boundary layers were observed in the inner region.

The general conclusion drawn from the observations is as follows. When the disturbance introduced into the flow field is two-dimensional, the transition process of vortex pairing is strongly two-dimensional. When the disturbance is not strongly organized, the transition may be weakly three-dimensional, but the mechanism of vortex pairing dominates the transition process. Therefore, transition in a wall jet flow is more like the vortex pairing mechanism for shear layers identified by Winant & Browand (1974) than the three-dimensional mechanism identified by Knapp & Roache (1968) for wall boundary layers. While multiple pairings were observed (very infrequently) in the present experiments, the transition to turbulence occurs after the first mature-stage coalescence, and will only be hastened by the occurrence of multiple pairings. The development of a three-dimensional transition pattern from a strongly organized two-dimensional disturbance, which is characteristic of the wall boundary layer, was not observed in the present experiments.

5.5. *Comparison with linear stability*

Quantitative data for the linear range of transition was reduced from the high-speed 16 mm films. The dimensionless wavenumber $\alpha^* = \alpha\delta$, the dimensionless convection velocity $c^* = C/U$, and the dimensionless frequency $f^* = f\delta/U$ for

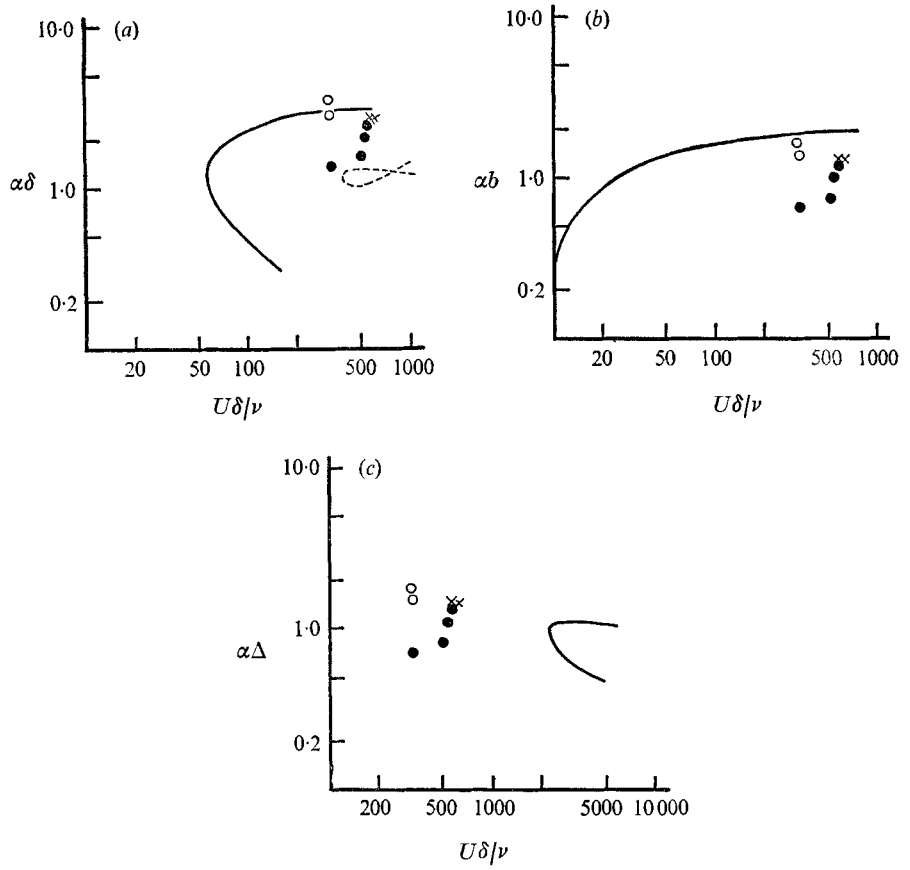

FIGURE 11. Dimensionless wavenumber plotted against the local wall jet Reynolds number $U\delta/\nu$. (*a*) $\alpha\delta$. ——, neutral curve for wall jet, first mode; – – – –, neutral curve for wall jet, higher mode. (*b*) αb, where b is the half-breadth of the outer shear layer. ——, neutral curve for plane free jet. (*c*) $\alpha\Delta$, where Δ is the thickness of the inner shear layer. ——, neutral curve for flat-plate boundary layer. ○, stable; ×, not clear; ●, unstable.

the wall jet boundary layer are presented in figures 11(*a*), 12 and 13(*a*), respectively. The solid curve is the result of Chun & Schwarz for the first-mode neutral solution of the Orr–Sommerfeld equation for the wall jet; and the dashed curve is the neutral solution for a higher mode. The solid data symbols denote cases where the disturbance was of sufficient magnitude that the boundary layer became unstable. The cross data symbols denote cases where it was not clear, for the limited field of view on the films, if the flow downstream from the observation point would have undergone transition to turbulence. Open data symbols denote observations judged to be stable. The data is correlated against the local Reynolds number $R_\delta = U\delta/\nu$. The present observations are in good qualitative agreement with the linear stability analysis calculations. Included with the dimensionless frequency data of the present investigators on figure 13(*a*) is the correlation of Bajura & Szewczyk, as represented by five data points. Their correlation was reduced to the relation $f^* = 0{\cdot}118$, for the local Reynolds

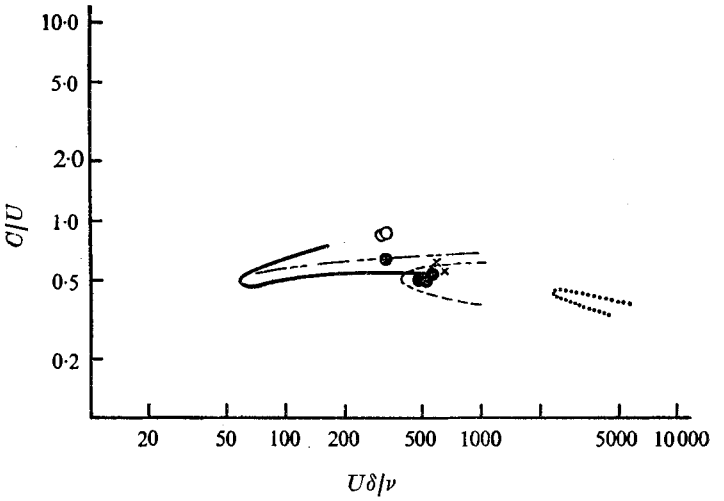

FIGURE 12. Dimensionless wave speed $c^* = C/U$ plotted against the local wall jet Reynolds number $U\delta/\nu$. ——, neutral curve for wall jet, first mode; – – – –, neutral curve for wall jet, higher mode; — – – —, neutral curve for plane free jet; · · · · ·, neutral curve for flat-plate boundary layer. ○, stable; ×, not clear; ●, unstable.

number range of 500–1200, and is therefore independent of the Reynolds number. It is interesting to note that their data for stable, neutral and amplified disturbances bear approximately the same relationship to the curve for the higher-mode disturbance as the present data bear to the first-mode disturbance. Their data were obtained at Reynolds numbers twice the value of the present results, and at nozzle-exit disturbance levels less than half the values of the present observations. The significance of the higher-mode neutral curve is not clear.

In view of the dual nature of the wall jet boundary layer, it is of interest to compare the dimensionless wavenumber, convection velocity and frequency data with the neutral curves of a plane free jet and the boundary layer along a flat plate. The comparisons for the plane free jet are presented on figures 11(*b*), 12 and 13(*b*), respectively, and the comparisons for the flat-plate boundary layer are presented on figures 11(*c*), 12 and 13(*c*) respectively.

In constructing these comparisons, some adjustments were made to the experimental data. For a plane free jet, the characteristic length is taken as the half-breadth b, which is defined as the distance from the point of maximum velocity to the point where the velocity is one half the maximum velocity. From the analytical solution of Glauert (1956), the half-breadth b is $0{\cdot}452\delta$, where δ is the previously defined wall jet boundary-layer thickness. Therefore, the dimensionless wavenumber αb for the plane free jet is $0{\cdot}452\alpha^*$; and the dimensionless frequency fb/U is $0{\cdot}452f^*$. These adjustments were made to the experimental data of figures 11(*a*) and 13(*a*) before they were plotted in figures 11(*b*) and 13(*b*), respectively. For the wall boundary layer, the characteristic length Δ is taken as the distance from the wall to the location where the velocity is 99 % of the free-stream velocity. This distance Δ is equal to $0{\cdot}548\delta$. Therefore, for the flat-plate boundary layer, the dimensionless wavenumber $\alpha\Delta$ is $0{\cdot}548\alpha^*$, and

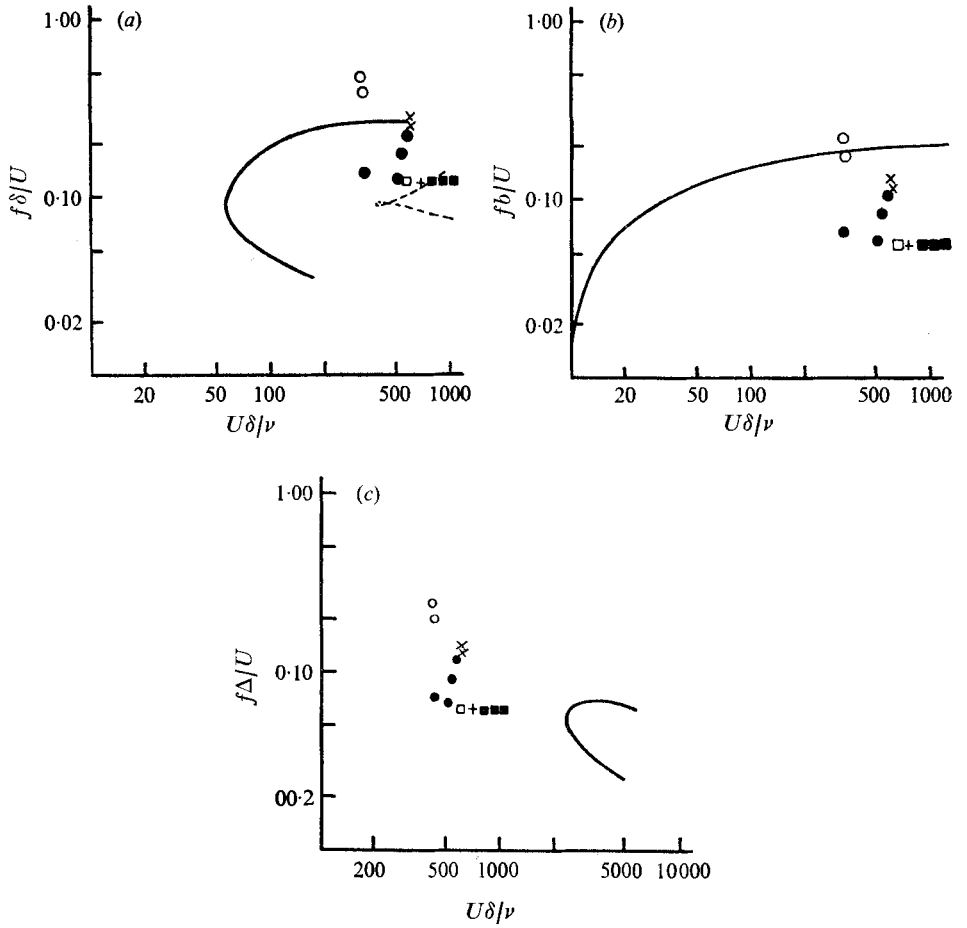

FIGURE 13. Dimensionless frequency plotted against the local wall jet Reynolds number $U\delta/\nu$. (*a*) $f\delta/U$. ——. neutral curve for wall jet, first mode; – – – –, neutral curve for wall jet, higher mode. (*b*) fb/U, where b is the half-breadth of the outer shear layer. ——, neutral curve for plane free jet. (*c*) $f\Delta/U$, where Δ is the thickness of the inner shear layer. ——, neutral curve for flat-plate boundary layer.

Present data	Bajura & Szewczyk	
○	□	Stable
×	+	Not clear
●	■	Unstable

the dimensionless frequency $f\Delta/U$ is $0{\cdot}548f^*$. These adjustments were made to the experimental data presented in figures 11(*c*) and 13(*c*) respectively. For both comparison flows, the dimensionless convection velocity C/U is equal to c^* for the wall jet flow, since the velocity scales are unchanged.

The curves shown on the figures are the neutral solutions for each flow considered. The analytical results for the plane free jet were taken from Tatsumi & Kakutani (1958). The Reynolds number Ub/ν for the plane free jet was increased by the factor (1/0·452), in order that the neutral curves could be presented in terms of the wall jet Reynolds number $U\delta/\nu$. The analytical solutions

for the wall boundary layer were taken from Schlichting (1960, pp. 169, 397). The local Reynolds number $U\Delta/\nu$ was increased by the factor (1/0·548), in order that these neutral curves could also be presented in terms of the wall jet Reynolds number.

These adjustments to both the experimental data and the analytical solutions to the linear stability equations enable the present wall jet data to be examined, with respect to each comparison flow, in terms of the characteristics for that flow only. If the inner and outer regions are considered as separate flow regimes, the outer region shows a great sensitivity to a given disturbance, whereas the inner region remains stable with respect to the disturbance. This result is in agreement with the previous conclusions, that the outer region controls the transition process.

6. Forced transition

The transition of the wall jet flow, when disturbed by acoustic fields, was completely dominated by the outer-region vortex-doubling process. An example of forced transition caused by acoustic disturbances is given by figure 14 (plate 3). In forced transition cases, the rolling-up of the flow into discrete vortices is more pronounced, and occurs close to the exit nozzle. Therefore, the energy available to the eddies is considerably greater than in the natural transition examples discussed previously, owing to the higher flow velocity for the same local Reynolds number. Figure 14(*a*) illustrates the doubling of two vortices in the outer region. The corresponding inner-region vortices are more pronounced than in the natural transition case. Figure 14(*b*) shows the rotation of the outer-region vortices around each other, and the beginning of the lift-off for the leading inner-region vortex. Figure 14(*c*) shows the penetration of the lifted-off jet into the ambient fluid. Note that the final stages of transition proceed rapidly from this last point, and no regions of non-turbulent flow exist downstream from the lift-off point. Downstream intermittency is eliminated completely. The exciting acoustic wave here corresponded to the frequency receiving the greatest amplification at a distance of 20 slit heights downstream from the exit nozzle (an 80 Hz wave). The complete transition process occurs in less than half the distance for natural transition. The deep penetration of the lifted-off flow into the ambient is not observed, and the turbulent wall jet remains on the plate.

Figure 15 illustrates the reaction of the wall jet to forced disturbances imposed by the loudspeaker system at five different frequencies. Calculations, using the correlation of Bajura & Szewczyk, predicted that a frequency of approximately 90 Hz would correspond to the most amplified disturbance near the exit from the channel nozzle. The lines connecting the circles in figure 15 represent the path followed by the wall jet in the R_δ, f^* plane as the flow moved downstream. Transition was markedly hastened when the disturbance was in the range 80–100 Hz. A 50% reduction in the transition length was noted, and all intermittency was removed from the transition process. At frequencies of 40 and 200 Hz, no apparent change in the natural transition process was observed. (The basic flow was unstable at this Reynolds number, and underwent transition

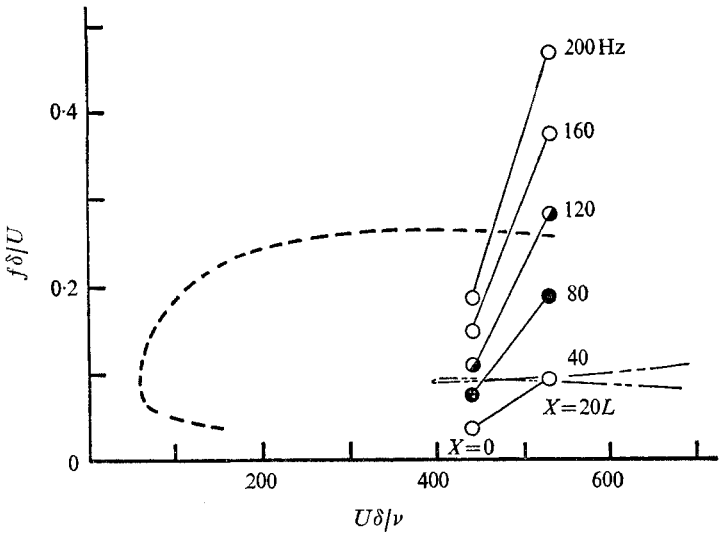

FIGURE 15. Sensitivity of wall jet to acoustic disturbances of various frequencies at an exit Reynolds number of 510. – – – – –, wall jet neutral curve, first mode; — — — — —, wall jet neutral curve, higher mode. ○—○, no change; ◑—◑, slight change; ●—●, marked change.

further downstream.) These experiments demonstrated that the wall jet is most sensitive to disturbances introduced into the entrainment shear layer at the nozzle exit, when the disturbance coincides with the characteristic frequency for the local critical Reynolds number.

7. Concluding remarks

7.1. *Initial disturbances*

The natural disturbances observed in the present experiments were so named because they could not be identified as originating from a known organized stimulus, such as acoustic excitation or seismic vibrations. Careful control of both the flow in the test facility itself and in the environment is required. Bajura & Szewczyk (1970) used similar precautions in their experiments with air, which included both the elimination of background noises in and around the room in which the test facility was located, and the motion of air currents near the working test section. The strength of disturbances in the exit flow of their experiments could not be measured, since the hot-wire signal level was equivalent to the noise level in the equipment (equivalent turbulence level less than 0·06 %). When any forcing was introduced, the wall jet became turbulent immediately downstream from the exit, as was observed in the present experiments. Unless background disturbances are controlled to low levels (which makes them difficult to measure), laminar wall jet flow either may not be observed, or will occur for only short distances. (See e.g. Newman 1961; Mon 1970.) The long natural transition lengths, obtained with the present channel nozzle, indicate that no strong organized disturbances were present in the laminar wall jet flow field.

7.2. *Influence of Reynolds number on transition*

Despite the wide variation in transition length for the jet and channel nozzles, the relative influence of the Reynolds number on transition was the same for either design. For low Reynolds numbers, in the range 75–200, the viscous effect of the inner region was a stabilizing influence on the entire flow field. Vortex pairings in the outer region were suppressed, while the rolling-up of the inner region became more pronounced. Under some conditions with the channel nozzle, the dye streaks entered the outflow collector without mixing (a distance of 640 slit heights). Transition in high Reynolds number wall jets (exit Reynolds numbers greater than 600) was completely dominated by the vortex-pairing process. Qualitative results, obtained from the high-speed films, indicate a periodicity in the flow which may correlate with the frequency of vortex pairings, as suggested by Winant & Browand. Transition characteristics in the exit Reynolds number range 200–600 were described in detail in previous sections. The numerical ranges of the exit Reynolds number, with respect to the associated transition characteristics, are not rigidly defined, and must be interpreted in terms of the location downstream from the nozzle where the disturbance is introduced. Close to the exit, more energy is available to the eddy system and, therefore, the outer region exerts more influence on transition (jet nozzle) than if the transition occurred further downstream (channel nozzle) for the same exit Reynolds number. As a result, the Reynolds numbers ranges for each nozzle were not coincident, owing to the spatial variations in the beginning of transition.

7.3. *Other experiments*

Experiments were conducted by Fales (1955) to examine transition in a wall boundary layer. The flow in Fales' experiments was produced by moving a flat plate through a tank of still water, and photographing the behaviour of dye streaks from an observation post mounted on a carriage travelling with the plate. Photographic records were also obtained while the plate was in the process of deceleration at the end of the test run. During periods of deceleration, the velocity profile along the plate surface is similar to the wall jet profile, in that there is an inner wall layer and an outer shear layer with a point of inflexion in the velocity profile. Fales reported observations of both clockwise and counter-clockwise vortex rolls for different plate speeds. These observations by Fales are in agreement with the present results, showing opposite rotation of the vortices in the inner and outer shear layers. A spanwise wavelike structure was also noted by Fales during the diffusive portions of the transition process for the vortex rolls, similar to the observations of the present study in stage (iv). It is postulated that the reason why Fales did not recognize the flow behaviour observed by the present investigators is that the dye streaks were introduced at fixed locations above the plate and, as the plate speed changed, the dye streaks were in different relative locations in the velocity profile. In view of the observations of Fales and the transitions studied with the channel nozzle where disturbances arose in the downstream flow field, it is concluded that the dual

shear-layer behaviour observed there is characteristic of the velocity profile, and not a function of the characteristics of the exit nozzle.

The authors are appreciative of the support, assistance and encouragement extended by Professor H. W. Butler, L. L. Blatt and O. E. McCoy during the research programme. The financial assistance of West Virginia University and the Babcock and Wilcox Research and Development Center is gratefully acknowledged.

REFERENCES

BAJURA, R. A. 1967 An experimental investigation of a laminar two-dimensional plane wall jet. Ph.D. thesis, University of Notre Dame, Notre Dame, Indiana.

BAJURA, R. A. & SZEWCZYK, A. A. 1970 Experimental investigation of a laminar two-dimensional plane wall jet. *Phys. Fluids*, **13**, 1653–1664.

BEAVERS, G. S. & WILSON, T. A. 1970 Vortex growth in jets. *J. Fluid Mech.* **44**, 97–112.

BROWAND, F. K. 1966 An experimental investigation of the instability of an incompressible, separated shear layer. *J. Fluid Mech.* **26**, 281–307.

BROWN, F. N. M. 1965 The physical model of boundary-layer transition. *David Taylor Model Basin, U.S. Navy, Contract*, no. 1623.

CATALANO, M. R. 1971 An experimental investigation of a plane wall jet. M.S. thesis, West Virginia University, Morgantown, West Virginia.

CHUN, D. H. & SCHWARZ, W. H. 1967 Stability of the plane incompressible viscous wall jet subjected to small disturbances. *Phys. Fluids*, **10**, 911–915.

FALES, E. N. 1955 A new laboratory technique for investigation of the origin of fluid turbulence. *J. Franklin Inst.* **259**, 491–518.

FREYMUTH, P. 1966 On transition in a separated laminar boundary layer. *J. Fluid Mech.* **26**, 683–704.

GASTER, M. 1965 The role of spatially growing waves in the theory of hydrodynamic stability. *Progress in Aeronautical Science* (ed. D. Kuchemann and L. Sterne), vol. 6, pp. 251–270. Pergamon.

GLAUERT, M. B. 1956 The wall jet. *J. Fluid Mech.* **1**, 625–643.

HAMA, F. R. 1960 Boundary layer transition induced by a vibrating ribbon on a flat plate. *Proc. Heat Transfer and Fluid Mechanics Institute*, pp. 92–105. Stanford University Press.

HAMA, F. R., LONG, J. D. & HEGARTY, J. C. 1957 On transition from laminar to turbulent flow. *J. Appl. Phys.* **28**, 388–394.

HAMA, F. R. & NUTANT, J. 1963 Detailed flow-field observations in the transition process in a thick boundary layer. *Proc. Heat Transfer and Fluid Mechanics Institute*, pp. 77–93. Stanford University Press.

KLEBANOFF, P. S., TIDSTROM, K. D. & SARGENT, L. M. 1962 The three-dimensional nature of boundary-layer instability. *J. Fluid Mech.* **12**, 1–34.

KNAPP, C. F. & ROACHE, P. J. 1968 A combined visual and hot-wire anemometer investigation of boundary-layer transition. *A.I.A.A. J.* **6**, 29–36.

KOVASZNAY, L. S. G., KOMODA, H. & VASUDEVA, B. R. 1962 Detailed flow field in transition. *Proc. Heat Transfer and Fluid Mechanics Institute*, pp. 1–26. Stanford University Press.

LINDOW, B. & GREBER, I. 1968 Similarity solution for a laminar incompressible jet flowing along a curved surface. *A.I.A.A. J.* **6**, 1331–1335.

MON, G. 1970 Two-dimensional incompressible laminar and turbulent curved wall jet. Ph.D. thesis, The Catholic University of America, Washington, D.C.

NEWMAN, B. G. 1961 The deflection of plane jets by adjacent boundaries – coanda effects. *Boundary Layer and Flow Control* (ed. G. V. Lachman), vol. 1, pp. 232–264. Pergamon.

PARKS, E. K. & PETERSEN, R. E. 1968 Analysis of a 'coanda' type flow. *A.I.A.A. J.* **6**, 4–7.

REDDY GORLA, R. S. & JENG, D. R. 1972 Laminar plane wall jet. *Proc. 12th Midwestern Mechanics Conf. Developments in Mechanics*, vol. 6, pp. 137–151. University of Notre Dame Press.

ROCKWELL, D. O. & NICCOLLS, W. O. 1972 Natural breakdown of planar jets. *Trans. A.S.M.E. J. Basic Engng*, **94**, 720–730.

SATO, H. 1956 Experimental investigation on the transition of laminar separated layer. *J. Phys. Soc. Japan*, **11**, 702–709.

SATO, H. 1959 Further investigation on the transition of two-dimensional separated layer at subsonic speeds. *J. Phys. Soc. Japan*, **14**, 1797–1810.

SATO, H. 1960 The stability and transition of a two-dimensional jet. *J. Fluid Mech.* **7**, 53–80.

SATO, H. & SAKAO, F. 1964 An experimental investigation of the instability of a two-dimensional jet at low Reynolds numbers. *J. Fluid Mech.* **20**, 337–352.

SCHLICHTING, H. B. 1960 *Boundary-layer Theory*, 4th edn. McGraw-Hill.

TATSUMI, T. & KAKUTANI, T. 1958 The stability of a two-dimensional laminar jet. *J. Fluid Mech.* **4**, 261–275.

TETERVIN, N. 1948 Laminar flow of a slightly viscous incompressible fluid that issues from a slit and passes over a flat plate. *N.A.C.A. Tech. Note*, no. 1644.

WINANT, C. D. & BROWAND, F. K. 1974 Vortex pairing: the mechanism of turbulent mixing-layer growth at moderate Reynolds number. *J. Fluid Mech.* **63**, 237–255.

WYGNANSKI, I. J. & CHAMPAGNE, F. H. 1968 The laminar wall jet over a curved surface. *J. Fluid Mech.* **31**, 459–465.

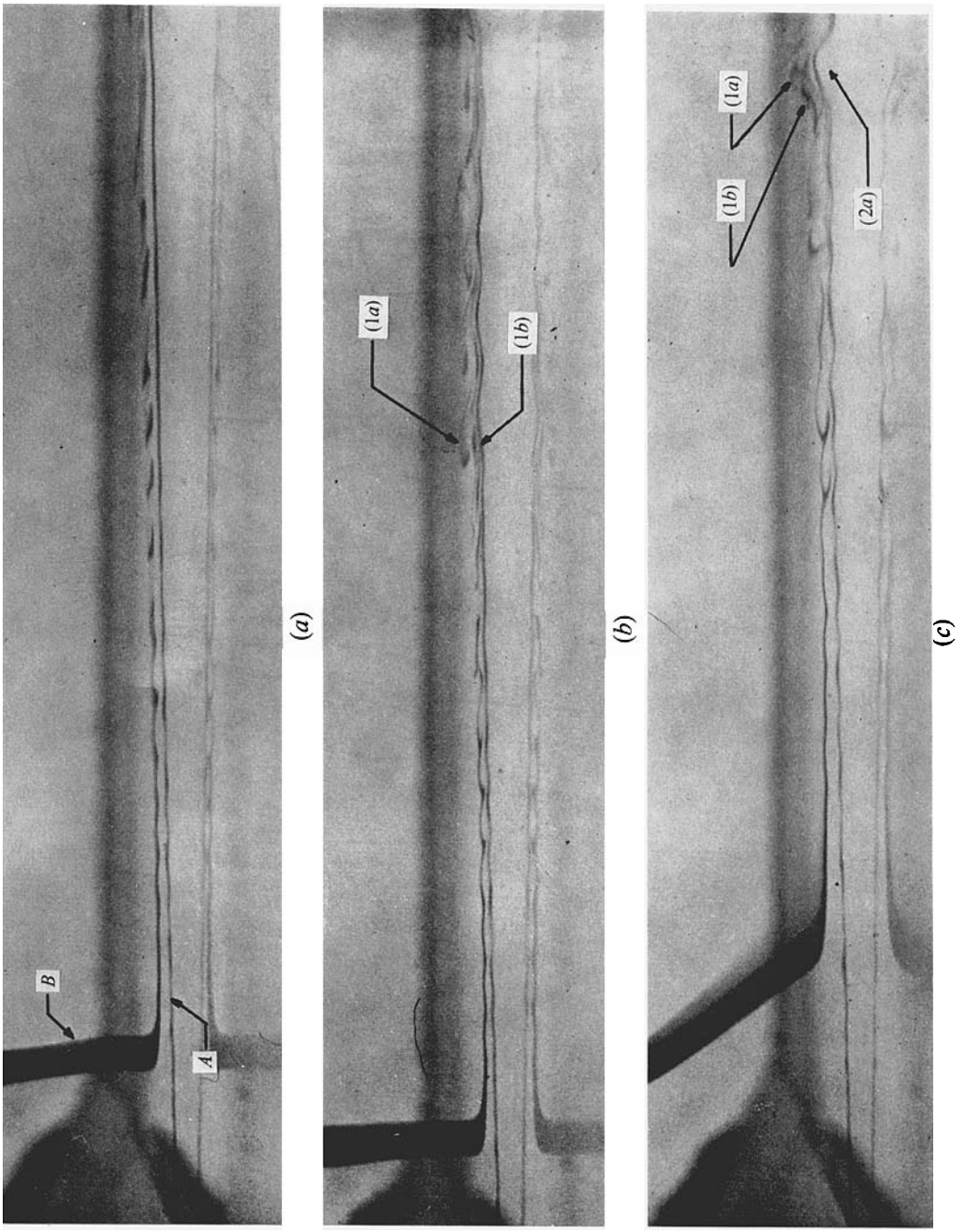

FIGURES 9 (*a–c*). For legend see plate 2.

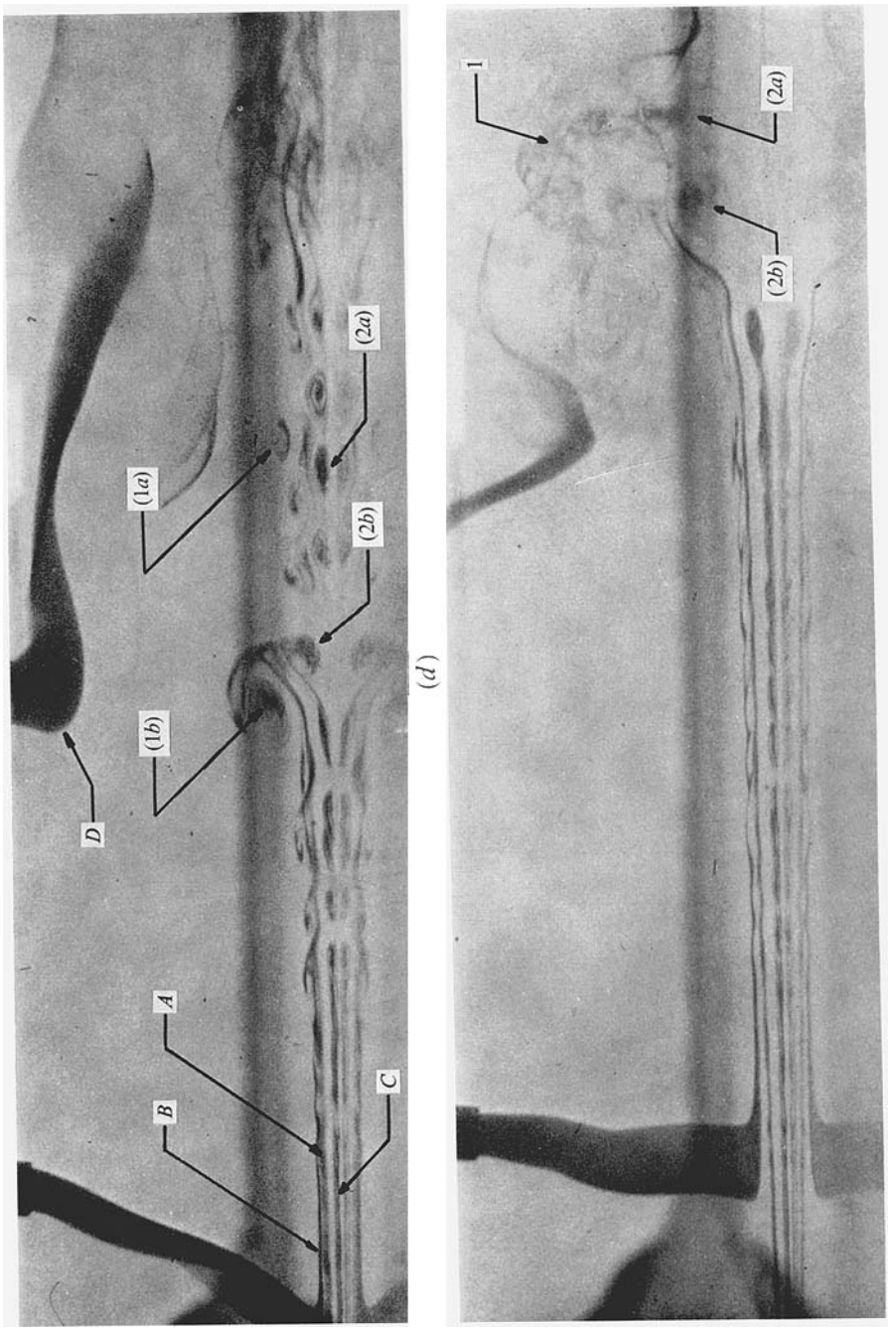

FIGURE 9. Photographs of dye streaks during transition for an exit Reynolds number of 5140. ((1) denotes outer region; (2) denotes inner region. Lower images are reflexions from plate surface.

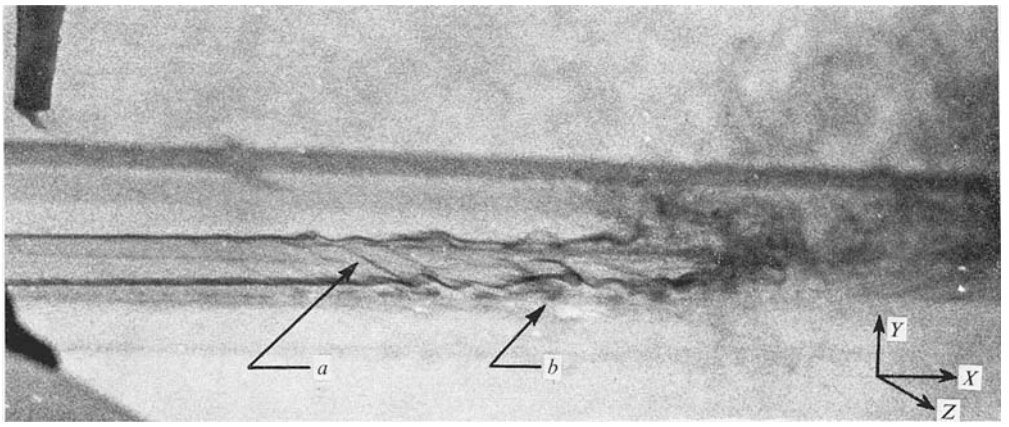

FIGURE 10. Spanwise view of dye streaks during transition for an exit Reynolds number of 384.

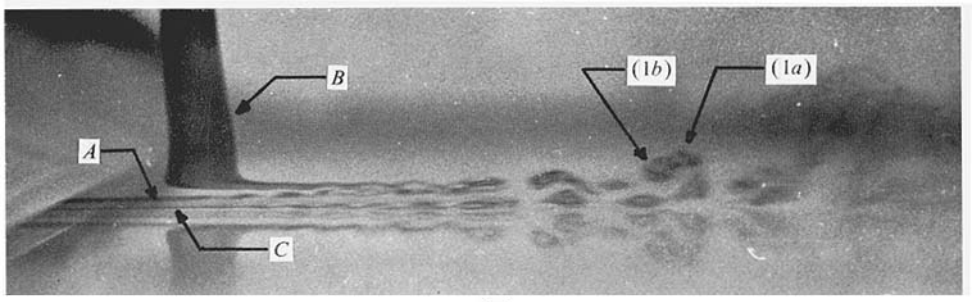

(*a*)

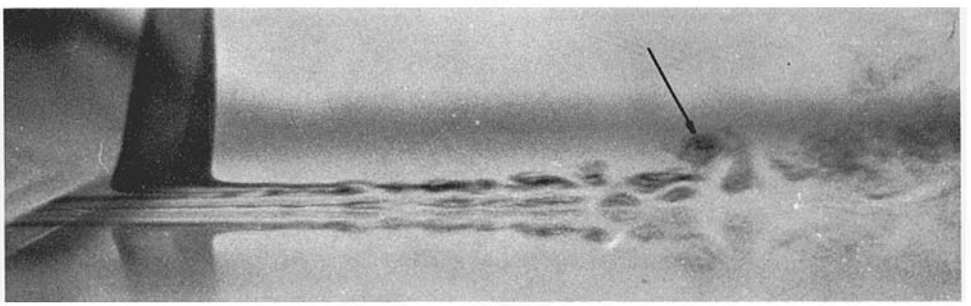

(*b*)

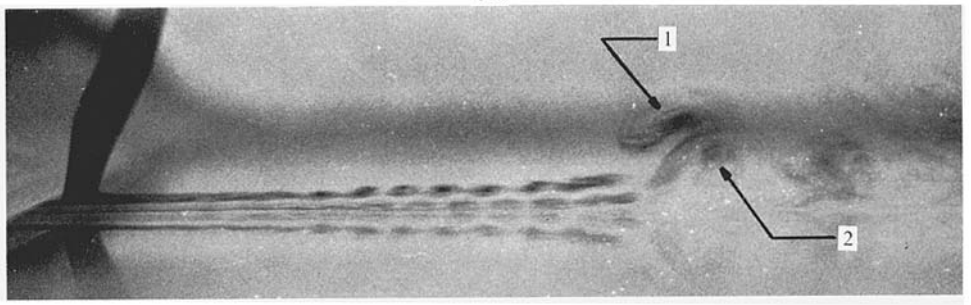

(*c*)

FIGURE 14. Photographs of dye streaks during forced transition due to acoustic disturbances at an exit Reynolds number of 510. Lower images are reflexions from plate surface.